Mon. Not. R. Astron. Soc. **294,** 229–244 (1998)

Testing deprojection algorithms on mock angular catalogues: evidence for a break in the power spectrum

E. Gaztañaga[1,2] and C. M. Baugh[3]

[1]*Institut d'Estudis Espacials de Catalunya, Research Unit (CSIC), Edf. Nexus-104 - c/Gran Capitan 2-4, 08034 Barcelona*
[2]*Department of Physics, Keble Road, Oxford OX1 3RH*
[3]*Department of Physics, Science Laboratories, South Road, Durham DH1 3LE*

Accepted 1997 September 5. Received 1997 August 15; in original form 1997 April 28

ABSTRACT

We produce mock angular catalogues from simulations with different initial power spectra to test methods that recover measures of clustering in three dimensions, such as the power spectrum, variance and higher order cumulants. We find that the statistical properties derived from the angular mock catalogues are in good agreement with the intrinsic clustering in the simulations. In particular, we concentrate on the detailed predictions for the shape of the power spectrum, $P(k)$. We find that there is good evidence for a break in the galaxy $P(k)$ at scales in the range $0.02 < k < 0.06\ h\ \mathrm{Mpc}^{-1}$, using an inversion technique applied to the angular correlation function measured from the APM Galaxy Survey. For variants on the standard cold dark matter (CDM) model, a fit at the location of the break implies $\Omega h = 0.45 \pm 0.10$, where Ω is the ratio of the total matter density to the critical density, and Hubble's constant is parametrized as $H_0 = 100\ h$ km s^{-1} Mpc^{-1}. On slightly smaller, though still quasi-linear scales, there is a feature in the APM power spectrum where the local slope changes appreciably, with the best match to CDM models obtained for $\Omega h \simeq 0.2$. Hence the location and narrowness of the break in the APM power spectrum combined with the rapid change in its slope on quasi-linear scales cannot be matched by any variant of CDM, including models that have a non-zero cosmological constant or a tilt to the slope of the primordial $P(k)$. These results are independent of the overall normalization of the CDM models or any simple bias that exists betwen the galaxy and mass distributions.

Key words: surveys – galaxies: general – dark matter – large-scale structure of Universe.

1 INTRODUCTION

Angular catalogues of galaxy positions provide us with powerful constraints on theories of structure formation in the Universe. The APM Galaxy Survey covers 4300 deg^2 on the sky and contains over 2 million galaxies to a limiting apparent magnitude of $b_J \leq 20.5$ (Maddox et al. 1990a,b,c, 1996). The shape of the angular correlation function measured from the survey at scales of $\theta > 1°$ indicates that the Universe contains more structure on large scales than is predicted by the standard cold dark matter (CDM) scenario (Maddox et al. 1990c).

Whilst this result is confirmed by the largest redshift surveys currently available (e.g. Efstathiou et al. 1990a; Saunders et al. 1991; Vogeley et al. 1992; Fisher et al. 1993; Tadros & Efstathiou 1996), measurements of correlations in 3D catalogues are still noisy on scales $r \geq 10\ h^{-1}$ Mpc. Only after the completion of the Sloan Digital Sky Survey (Gunn & Weinberg 1995) will a 3D catalogue contain the same order of magnitude of objects as the APM Galaxy Survey.

An additional complication in redshift catalogues is that the pattern of galaxy clustering is distorted by the peculiar motions of galaxies (Kaiser 1987). This effect can boost the amplitude of the measured two-point correlations by a factor anywhere in the range 1–2 on large scales, depending upon the survey and the method of analysis (see table 1 in Cole, Fisher & Weinberg 1995).

Whilst the next generation of redshift surveys will undoubtedly provide a wealth of new information that is not available in angular catalogues, it is important to take full advantage of the large number of galaxies and volume surveyed in the angular catalogues (such as the APM Survey and the parent catalogue for the Sloan Survey when it is complete) to extract information about the correlations on large scales. Under certain assumptions, deprojection algorithms to recover the 3D correlations and real space have been developed for multipoint correlation functions (e.g. Groth & Peebles 1977; Fry & Peebles 1978; Peebles 1980), for *J*-order cumulants of counts in cells (Gaztañaga 1994, 1995, hereafter G94 and G95) and for the power spectrum (Baugh & Efstathiou 1993, 1994, hereafter BE93 and BE 94). In this paper we present tests of these algorithms by constructing angular catalogues, with the same selection function and angular mask as the APM catalogue, from large numerical simulations. We use sets of simulations that have been evolved to have a 3D power spectrum that matches closely the APM form recovered by BE93 and also simulations of CDM models.

For our present purposes, we are concerned with testing for the presence of any systematic biases that arise from the projection process itself rather than from the actual construction of the APM Survey or corresponding angular catalogue (some of these problems are addressed in detail by Maddox et al. 1996).

The outline of the paper is as follows. In Section 2 we describe the *N*-body simulations used to make mock catalogues in Section 3. We present and test the recovery methods in Sections 4 and 5. In Section 6 we discuss our results and present the conclusions.

2 *N*-BODY REALIZATIONS OF APM GALAXY CLUSTERING

A discussion of the production of evolved *N*-body simulations that have the same power spectrum as that measured for APM Survey galaxies (BE93; BE94) is given in Baugh & Gaztañaga (1996, hereafter BG96). In this section we briefly summarize the approach taken and list the parameters of the *N*-body simulations that are used to make mock APM catalougues in Section 3.

The first step is to estimate the linear power spectrum from the measured power spectrum of APM Survey galaxies. This requires assumptions to be made about the cosmological model and the form of the bias, if any, between fluctuations in the light and the mass distributions (Kaiser 1984). In this paper we consider a spatially flat universe with the critical density $\Omega=1$ and zero cosmological constant. We assume that there is no bias between light and mass, i.e., that light traces mass, for simplicity. The validity of this assumption is not important for the purposes of this paper, which are to generate a particular distribution of points in 3D and to determine how well the *N*-point correlations in 3D can be recovered from a projected catalogue. There is evidence that the relative bias between mass and light is small on large scales from the hierarchical scaling of higher order moments of galaxy counts in the APM Survey (G94), although this does not appear to be the case on smaller scales (BG96).

The linear power spectrum is obtained from the evolved power spectrum using the transformation of Jain, Mo & White (1995). This transformation is based upon a suggestion by Hamilton et al. (1991) that a universal form exists relating the linear and non-linear correlation functions. The method was extended to power spectra by Peacock & Dodds (1994), and modified by Jain et al. (1995) to cope with steep power-law fluctuation spectra, $P(k)\propto k^n$, with $n<-1$. We have found that the formula of Jain et al. gives more self-consistent results for the $n\sim -2$ linear power spectra discussed here than the revised formula given by Peacock & Dodds (1996).

The linear to non-linear transformation is given by

$$\Delta^2(K_{\rm NL})/b(n)=f_{\rm NL}[\Delta^2_{\rm L}(k_{\rm L})/b(n)], \quad (1)$$

$$k_{\rm L}=[1+\Delta^2_{\rm NL}(k_{\rm NL})]^{-1/3}k_{\rm NL}, \quad (2)$$

where the subscripts L and NL refer to linear and non-linear respectively, and $\Delta(k)=4\pi k^3P(k)/(2\pi)^3$ is the fraction variance of the density field in bins of $\ln k$. The factor $b(n)=[(3+n)/3]^{1.3}$ is a function of the effective spectral index of the density fluctuations, defined as the local slope of the linear power spectrum at the scale on which the variance is unity. Using the functional form for the inverse of $f_{\rm NL}$ given by equation 7(b) of Jain et al. (1996), the linear power spectrum corresponding to the measured APM galaxy power spectrum can be calculated iteratively. The linear APM power spectrum is shown by the solid line in Fig. 1, with the measured APM galaxy power spectrum shown by the open circles. The error bars show the 1σ scatter in the mean from averaging over the APM Survey split up into four zones (BE93; BE94). The linear APM power spectrum is smoother than the measured spectrum

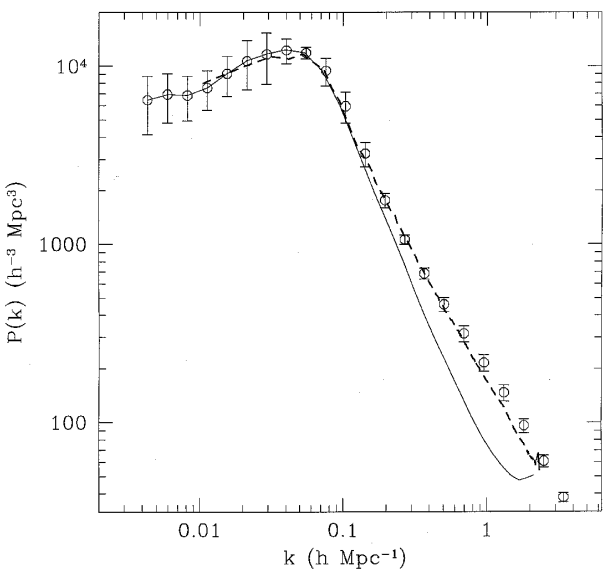

Figure 1. The power spectrum measured for APM Survey galaxies is shown by the open circles with the 1σ scatter on the mean, averaged over the survey split up into four zones. The solid line shows the linear power spectrum estimated from this, as described in the text. The dashed line shows the power spectrum measured from the evolved simulation, APM2(a).

and is better fitted by a simple analytic form: for $k < 0.6\ h$ Mpc^{-1},

$$P_{\rm APM}(k) \propto \frac{k}{[1+(k/k_{\rm c})^2\}^{3/2}}, \qquad (3)$$

with $k_{\rm c} \approx 150\ H_0/c$ (BG96).

The linear APM power spectrum is used to generate the initial density fluctuations in an N-body simulation. The simulation is evolved until the variance measured in spheres of radius 30 h^{-1} Mpc matches that in the APM Survey. Several sets of simulations with APM initial conditions are used in this paper. APM1 consists of one simulation with 160^3 particles in a box with sides 440 h^{-1} Mpc. APM2 has one realization with 200^3 particles in a 600 h^{-1} Mpc box, and APM3 is an ensemble of five simulations (a)–(e), with half as many particles as APM1 and a slightly smaller box. The parameters of the simulations are listed in Table 1. The power spectrum of the evolved simulation APM2(a) is shown by the dashed line in Fig. 1. The evolved power spectra give a very close match to the measured APM power spectrum. In all cases, we generate the initial conditions using a fast Fourier transform (FFT) on a 256^3 potential grid ($N_{\rm g}=256$). The softening length of the APM3 and CDM3(a) runs was adjusted to be comparable to that used in the APM1 run. All simulations were run using the P^{3}M particle–particle/particle–mesh code of Efstathiou et al. (1985).

We have run two simulations with the same random phases as APM2(a) and APM3(a), but with the standard CDM power spectrum, $\Omega=1$ and $h=0.5$; these are called SCDM2(a) and SCDM3(a). We also ran another CDM simulation with the same random phases as APM3(a) and SCDM3(a), but with a low density parameter and a non-zero value of the cosmological constant, $\Omega=0.2$, $\Lambda=0.8$ and $h=1$, which is called LCDM3(a). The initial density field in the CDM simulations is set up using the transfer function of Bond & Efstathiou (1984) for a universe with baryon density $\Omega_{\rm B}=0.03$. This transfer function can be expressed in terms of a parameter $\Gamma=\Omega h$ (Efstathiou, Bond & White 1992); note that this definition of the shape parameter Γ is relative to a model with $\Omega_{\rm B}=0.03$ and differs slightly from that adopted by Peacock & Dodds (1994). In all cases we have run the CDM simulations so that the linear variance on scales of 8 h^{-1} Mpc is $\sigma_8 \simeq 0.84$ (note that this value does not take into account any evolution in the clustering, and corresponds to clustering at the mean redshift in the APM; e.g. G95). The SCDM simulation has more power on small scales and less power on large scales than the APM run. This can be seen in a comparison of the particle distributions from APM2(a) and SCDM2(a) shown in Fig. 2. The figure shows a slice from the simulation box, after the particle density has been tabulated on a 256^3 grid and smoothed on small scales with a Gaussian filter. The slice shown is ~ 3 h^{-1} Mpc square.

Table 1. Simulation parameters. The third column gives the dimension of the FFT mesh used in the long-range force calculation. The last column gives the softening length of the gravitational force, ϵ in h^{-1} kpc units.

run	number of particles	mesh	L_{box} $(h^{-1}Mpc)$	ϵ $(h^{-1}kpc)$
APM1	160^3	256^3	440	115
APM2(a)	200^3	256^3	600	156
APM3(a)-(e)	126^3	128^3	400	104
SCDM2(a)	200^3	256^3	600	156
SCDM3(a)	126^3	128^3	400	104
LCDM3(a)	126^3	128^3	400	104

3 MOCK APM MAPS

We transform the N-body simulation into a mock APM catalogue of angular positions by the following steps.

(i) Select an arbitrary point in the simulated box to be the local 'observer'.

(ii) Apply the APM Survey angular mask, including plate shapes and holes.

(iii) Include a simulated particle at coordinate distance x from the observer with probability given by the selection function $\psi(x)$.

The discreteness of the density field in the N-body simulations means that the final maps have a slightly lower density than the real APM map. The total number of particles is about 8×10^5 compared with 1.3×10^6 galaxies in the APM Survey to the same apparent magnitude limit. This introduces additional shot-noise in the measurements, which is corrected in the standard way (e.g. G94). The simulations use a periodic box, so we replicate the box to cover the total extent of the APM volume (over 1200 h^{-1} Mpc; beyond this the expected number of galaxies is of order unity). By comparing the results from different box sizes we have verified that this replication of the box does not introduce any spurious correlations on large scales.

3.1 The selection function

The selection function $\psi(x)$ is the normalized probability that a galaxy at coordinate distance x is included in the catalogue. This probability is proportional to the estimated number of galaxies at this coordinate:

$$\psi(x) = \psi^* \int_{q_1(x)}^{q_2(x)} {\rm d}q\ \phi(q), \qquad (4)$$

where ψ^* is adjusted so that the probability integrates to unity over the sample. $\phi(q)$ is the luminosity function, and $q_1(x)$ and $q_2(x)$ are the scaled luminosities corresponding to the lower and upper limits in the range of apparent magnitudes used to build the galaxy sample or catalogue under study. In our case these are $b_J=17$ and 20 respectively. G95 constructed a χ^2 test to find contours of the values of the luminosity function parameters that best fit observational constraints on the luminosity and redshift distribution; the redshift revolution of the luminosity function is parametrized as $\phi^*=\phi_0^*(1+\phi_1^* z)$; $\alpha=\alpha_0+\alpha_1 z$ and $M=M_0^*+M_1 z$. Here we use the best-fitting parameters obtained by G95: $\phi_1^*\sim 0$, $\alpha_1=-4$ and $M_*^1=-2$ and the zeroth-order values of Loveday et al. (1992): $\phi_0^*=0.0112\ h^3$ Mpc^{-3}, $M^*_0=-19.73$, $\alpha_0=-1.11$. BE93 proposed a functional form for the redshift distribution $N(z$, discussed below in Section

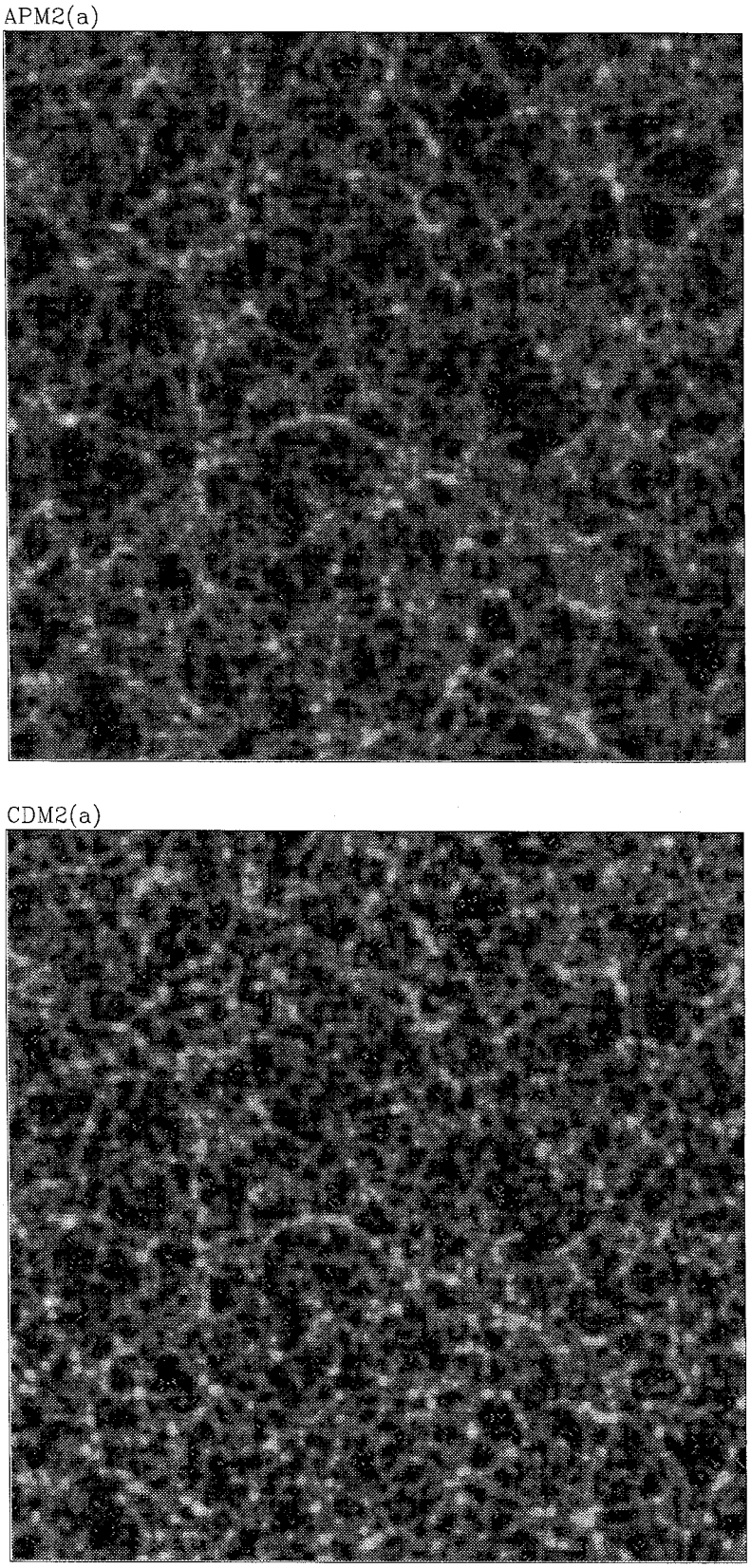

Figure 2. A comparison of the evolved density field in the APM2(a) (top) and CDM2(a) (bottom) simulations, which were started with the same random phases. The density is binned on a 256^3 grid, and is smoothed with a Gaussian filter to blur the pixels. The grey-scale shows the logarithm of the density. The slices are 3 h^{-1} Mpc thick and 600 h^{-1} Mpc square.

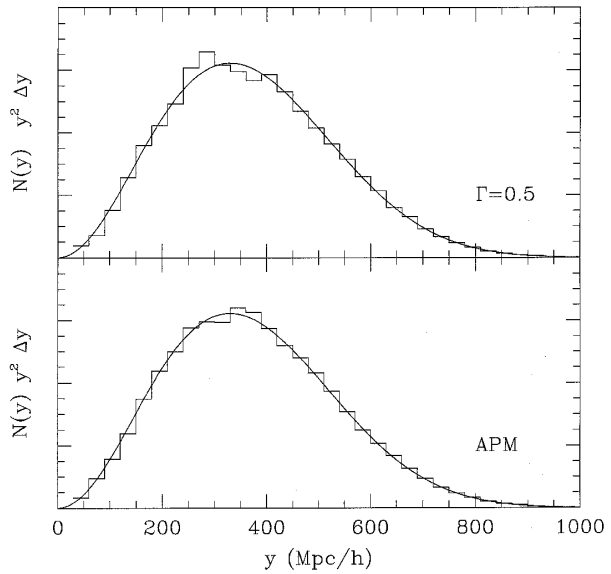

Figure 3. Comparison of the theoretical (smooth curve) and measured counts (histogram) in radial shells for two mock catalogues made from the simulations SCDM3(a) (top) and APM3(a) (bottom).

5. This $N(z)$ distribution gives very similar results for the selection function.

Fig. 3 shows a comparison between the expected number of galaxies, $n(y)\,y^2\Delta y$, at different radial depths (in comoving coordinates y) given by the input selection function compared to the measured counts for two different mock catalogues.

3.2 Equal-area projection maps

We have made equal-area projected maps from the mock catalogues. To facilitate a comparison between the maps made from the different simulations and the map of the APM Galaxy Survey, the maps have been turned into grey-scale plots shown in Fig. 4. Grey intensity increases as a low power ($\simeq 0.1$) of the point density. The mock catalogues are from the same realization of the random seeds, and therefore have the same fluctuations in the same places but with different amplitudes, given by the difference in the initial power spectrum and its subsequent non-linear evolution. In the notation of Table 2 these maps are from the simulations APM3(a), SCDM3(a) and LCDM3(a). The real APM map has been diluted to show the same mean surface density. The angular correlations are given in Figs 5 and 6. A visual comparison shows that the SCDM model does not have as strong large-scale fluctuations as the APM map, which is confirmed by Fig. 5 (as found earlier by Maddox et al. 1990c). The SCDM distribution is quite smooth on the largest scales. One can also see how both CDM models have larger fluctuations on the smallest scales in these maps, showing a distinctive granulation in grey-scale. The mock APM map is the closest of the models to the real catalogue, as expected from the very good agreement in the variance (cf. Fig. 5). Of course, the locations of individual structures in the real and mock APM maps do not coincide. Any statistical differences are due to differences in higher order correlations.

3.3 Angular correlations

Fig. 5 compares the variance $\bar{w}_2 = \langle \delta^2 \rangle_c$, of angular fluctuations δ in cells of radius θ. The angular variance in the APM Survey is shown by the points with error bars (G94). The lines show the variance in the mock catalogues made from the SCDM3(a) (short-dashed), LCDM3(a) (long-dashed) and APM3(a) (solid) simulations. The CDM mock catalogues all have, by construction, the same linear-theory normalization $\sigma_8 \simeq 0.84$, but the non-linear σ_8 is, of course, slightly different in each case. The simulated APM mock catalogue is slightly off the measured APM values around 2°–4°; this is also true for the mean different realizations, and is probably due to slight inaccuracies in the match of the evolved power spectrum in the simulation to the measured galaxy power spectrum. Note that all catalogues have similar power at around 1°. As expected, the LCDM model matches well the shape of the variance at larger scales, while the SCDM does not have enough large-scale power. At smaller scales the CDM models have too much power, as noted previously (e.g. Efstathiou, Sutherland & Maddox 1990b; G95; BG96).

Fig. 6 shows the skewness or third-order reduced cumulant $\bar{w}_3 = \langle \delta^3 \rangle_c$, for the same single realization of each model compared to the APM measurements. The errors show that at scales bigger than 1° there are very large sampling fluctuations in $\bar{w}_3$. This is more dramatic in single realizations of each mock catalogue that covers a smaller volume than the real APM. It is therefore dangerous to draw any conclusions, from this figure alone, at scales $\theta > 1°$. By comparing different realizations, we note that the mean at $\theta > 1°$ comes closer to the APM observations.

In the following two sections we first give a brief review of the deprojection algorithms; we then estimate the 3D statistics from the full simulation box, i.e. the $\bar{\xi}_J$ using the counts-in-cells method for the whole simulation box (as in Baugh, Gaztañaga & Efstathiou 1995) or the power spectrum. The 2D measurements of clustering, the $\bar{w}_J$ or the angular correlation function, are estimated from the mock catalogues (as in G94) and the deprojection algorithms described in the previous section are applied.

4 RECOVERY OF THE MOMENTS OF COUNTS IN CELLS

Here we use a simple method for recovering the 3D variance, $\bar{\xi}_2(R)$, and higher order reduced moments, $\bar{\xi}_J(R)$, from the 2D correlations, $\bar{w}_J(\theta)$. This method was introduced and applied to the APM Galaxy Survey in G94, G95, where a full description can be found.

In a scale-invariant model $\bar{\xi}_2 \propto R^{-\gamma}$ with slope γ, we can use the expressions in G95 to relate the estimated angular amplitudes to the underlying 3D amplitudes, i.e. $\sigma_8^2 \equiv \bar{\xi}_2(R=8)$ and $S_J \equiv \bar{\xi}_J/\bar{\xi}_2^{J-1}$. Here we consider a distribution that is not exactly scale-invariant, but has a slope γ which is a slowly varying function of scale. We call this a quasi-scale-invariant model (see G95). It is then possible to apply a local inversion at each scale. In principle, the correlations on all scales R contribute to the correlations on

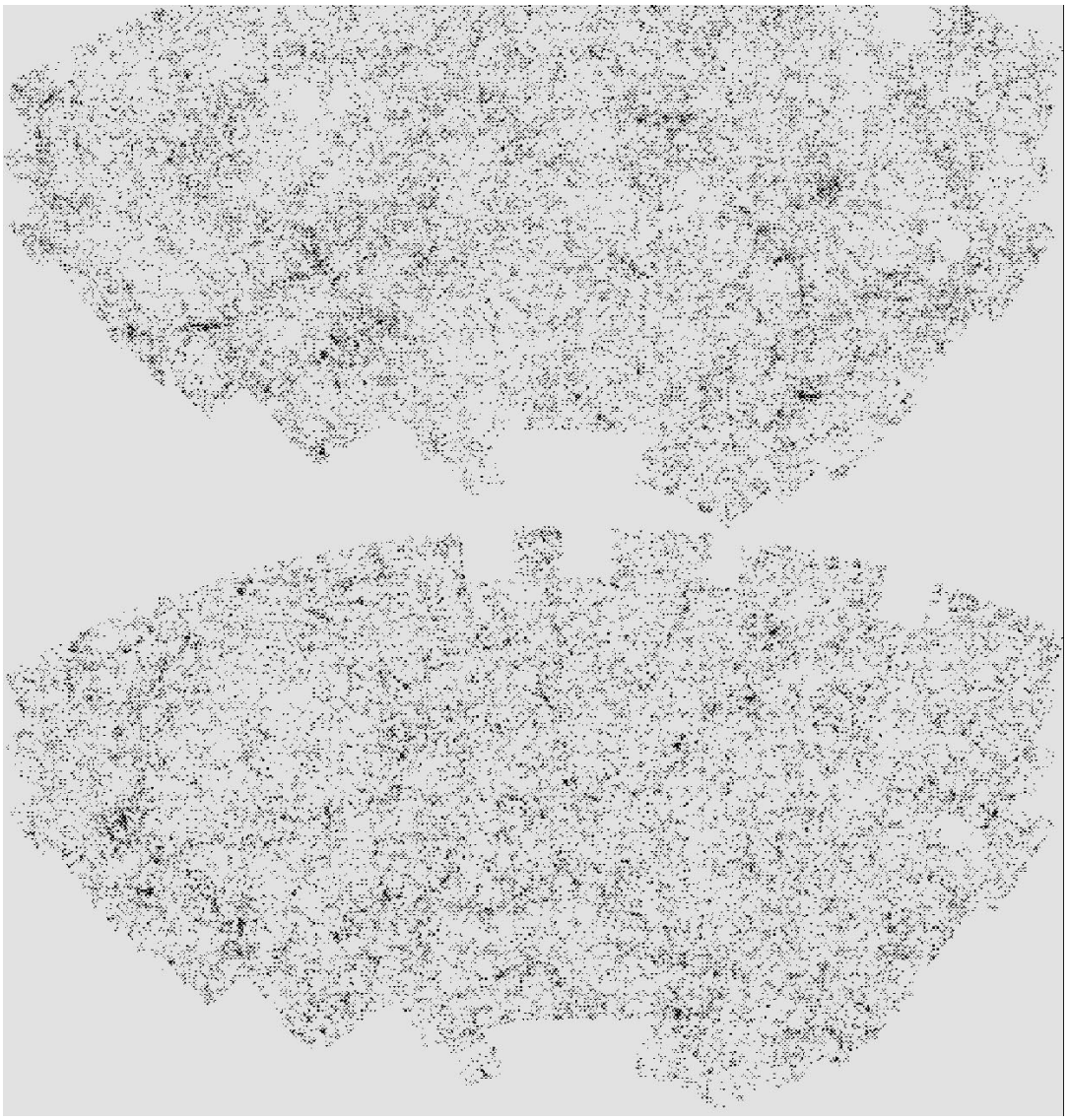

Figure 4. Comparison of equal-area projections of maps made from simulated catalogues with the real APM Galaxy Catalogue (Maddox et al. 1990a,b) (top). The surface density of galaxies is represented by a grey-scale, with the densest regions being the brightest. In each map, the same total number of galaxies and the same grey-scale calibration are used. The maps extend about 120° in RA and 60° in Dec., covering about 20 per cent of the Southern Galactic Cap, with a mean depth of 400 h^{-1} Mpc. The 185 overlapping square UK Schmidt plates in each map correspond roughly to 5° on a side. All maps have similar amplitudes of fluctuations ($\bar{w}_2$) at 1°. From top to bottom we show the real APM Survey, the standard CDM map made from SCDM3(a), a lambda-CDM map made from LCDM3(a), and a mock APM map made from a simulation [APM3(a)] evolved to match the power spectrum of APM galaxies.

angular scale θ, but because the sample has a finite depth, $\mathscr{D}$, there is a characteristic scale $R \simeq \mathscr{D}\theta$. In our analysis we relate angular scales θ to 3D scales using $R = \mathscr{D}\theta$, where $\mathscr{D}$ is the estimated distance which corresponds to the mean redshift of the sample (see also Peebles 1980). Although there is some ambiguity as to what the best definition of $\mathscr{D}$ should be, in the scale-invariant regime we find that the estimated amplitudes of $\bar{\xi}_J$ are insensitive to changes in our chosen value of $\mathscr{D}$.

Thus, at each given scale θ with local slope $\gamma = \gamma(\theta)$, we use the scale-invariant expressions to relate the estimated local angular amplitudes to the underlying 3D values. This results in an estimation for $\bar{\xi}_J$ as a function of the scale $R = \mathscr{D}\theta$. This model was used in G94 and G95 to recover the 3D correlations in the APM Survey.

4.1 Test of the variance

Fig. 7 shows the inversion of $\bar{\xi}_2(R)$ from a standard $\Gamma = \Omega h = 0.5$ CDM mock angular catalogue (right-hand panel), and for a mock APM catalogue (left-hand panel) compared to the corresponding variance $\bar{\xi}_2(R)$ estimated directly in the 3D simulation [e.g., SCDM3(a) and APM3(a)]. The variance recovered from the angular distribution is a very good match to the variance measured from the full simulation. There is a slight disagreement at

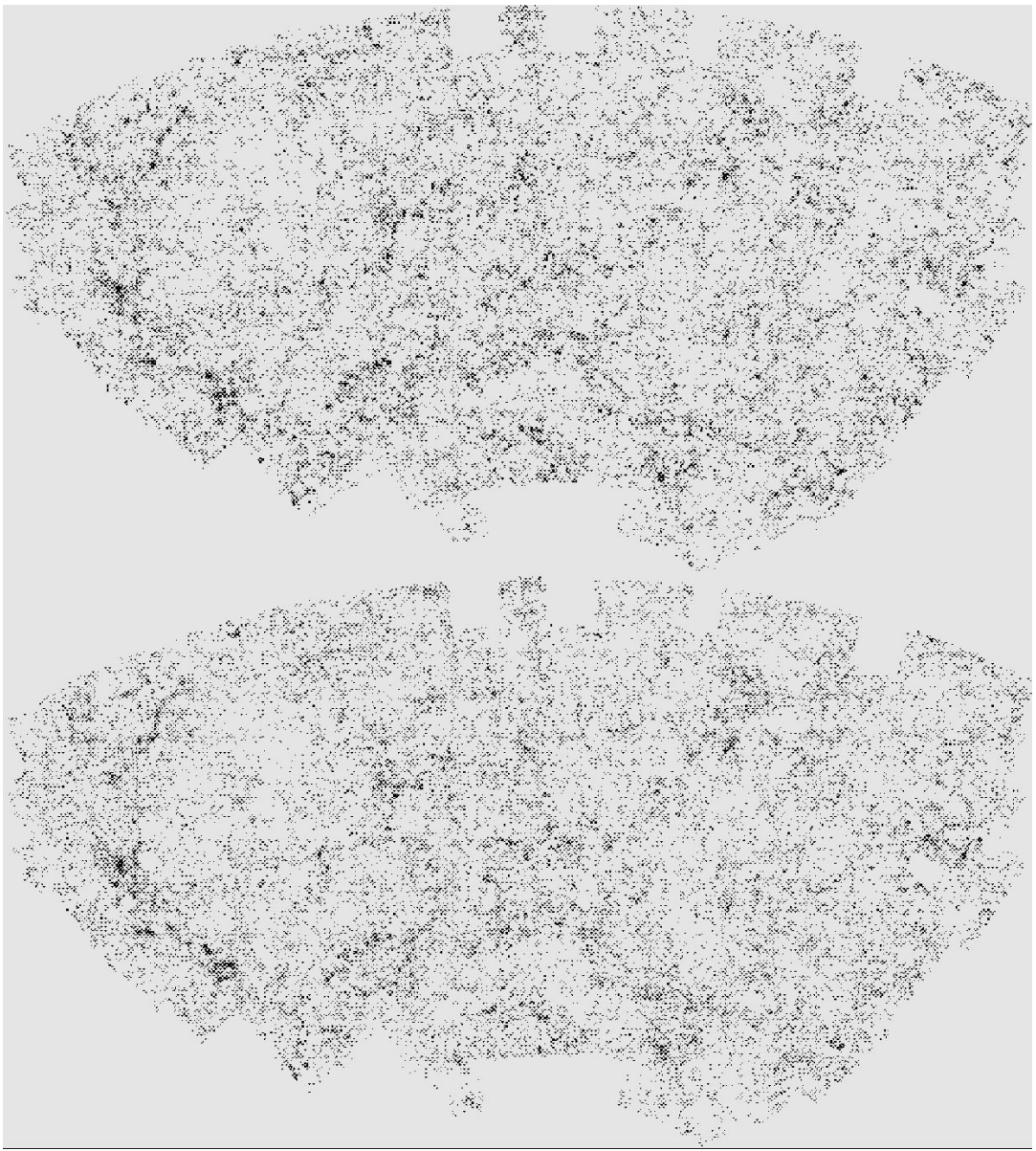

Figure 4 – *continued*

scales around $R \sim 20\,h^{-1}$ Mpc, where there is a rapid change in the slope, as expected, but the discrepancies are within 1σ.

4.2 Test of higher order moments

The simulations we use have values of S_J which show a small variation with scale, e.g. $S_3 \propto R^{-\alpha}$, with $\alpha \simeq 0.1$. This indicates that, strictly speaking, neither the scale-invariant nor the quasi-scale-invariant models should be used, as the S_J should be constants in the hierarchical model. Nevertheless, we still find reasonable agreement from the inversion when we compare local values of S_J.

Figs 8 and 9 show the inversion of $S_3(R)$ and $S_4(R)$ from the standard $\Gamma = 0.5$ CDM mock angular catalogue and for the APM-like mock catalogue compared to the corresponding amplitudes estimated directly in the 3D simulated box. At scales $20 > R > 6\ h^{-1}$ Mpc, the amplitudes recovered from the angular distribution are in good agreement with the original amplitudes. At larger scales, sampling fluctuations are very large, whereas at smaller scales, there are some systematic differences which seem more important for the APM model, which has a steeper power spectrum. As expected, the inversion method seems to work better for distributions where the S_J are closer to being constants, e.g., SCDM. Note that the measured amplitudes S_J in the APM are closer to a constant than either of the models we study here (G94; G95), and one would then expect an even better agreement in this case. The discrepancies at small scales could also be due in part to shot-noise in either the angular or the 3D distribution.

As was pointed out in Gaztañaga & Bernardeau (1997), there are several effects that make this type of comparison difficult. First, volume and boundary effects are important

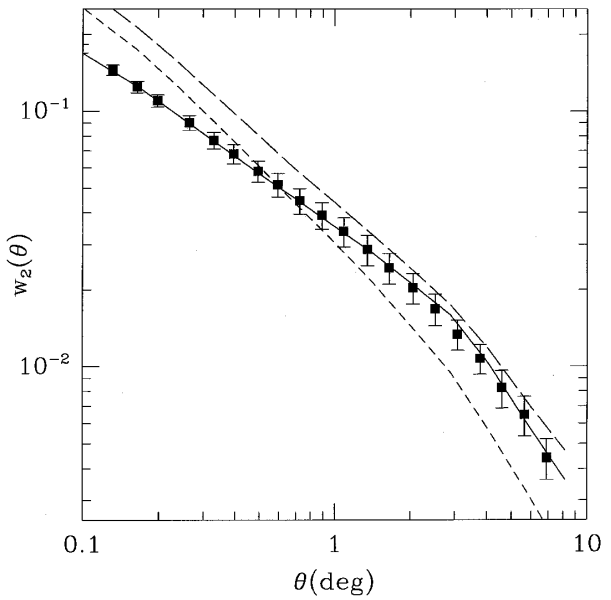

Figure 5. Comparison of variance of angular counts-in-cells, $\bar{w}_2(\theta)$, in the simulated mock catalogues with the results in the real APM data (symbols with error bars). Single realizations of the maps made from the SCDM3(a), LCDM3(a) and APM3(a) simulations, normalized to a linear variance of $\sigma_8=0.84$, are shown respectively as short-dashed, long-dashed and continuous lines.

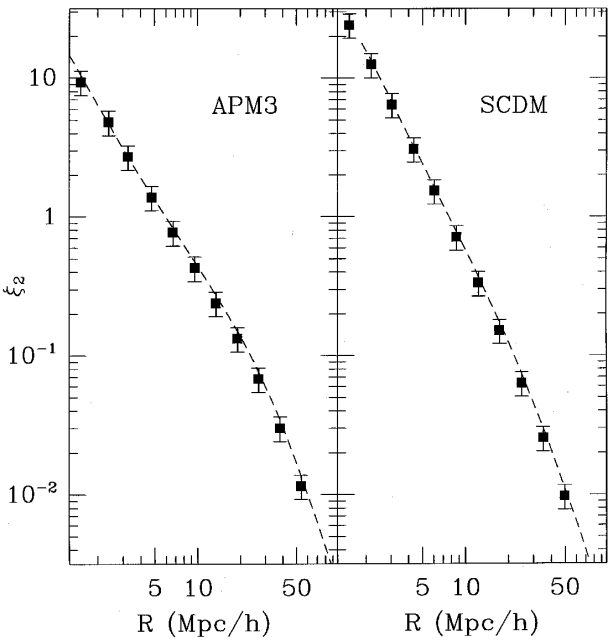

Figure 7. Comparison of variance of counts-in-cells, $\bar{\xi}_2(R)$, in the simulated box (lines) with the results inverted from the corresponding angular mock catalogue (points). The right-hand panel corresponds to the $\Gamma=0.5$ CDM model SCDM3(a), while the left-hand panel shows the results from the APM3(a) mock catalogue.

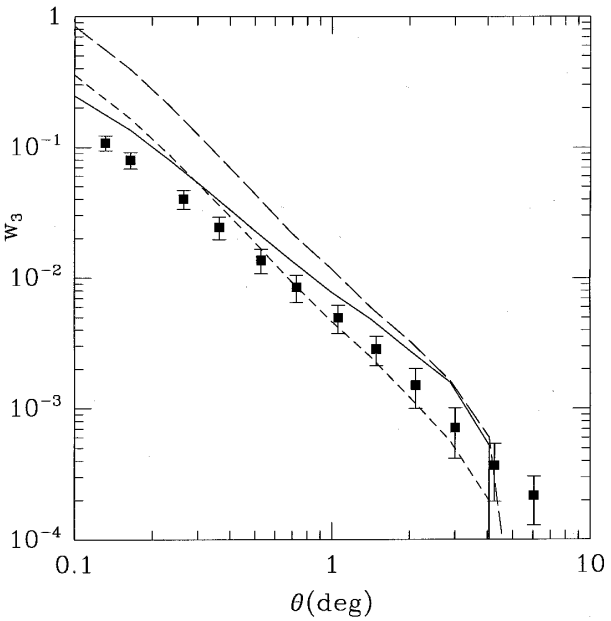

Figure 6. Comparison of the skewness $\bar{w}_3$ of angular counts-in-cells, in the simulated mock catalogues with the results in the APM Survey (symbols with error bars). The SCDM3(a), LCDM3(a) and APM3(a) simulations, normalized to linear $\sigma_8=0.84$, are shown respectively as short-dashed, long-dashed and continuous lines.

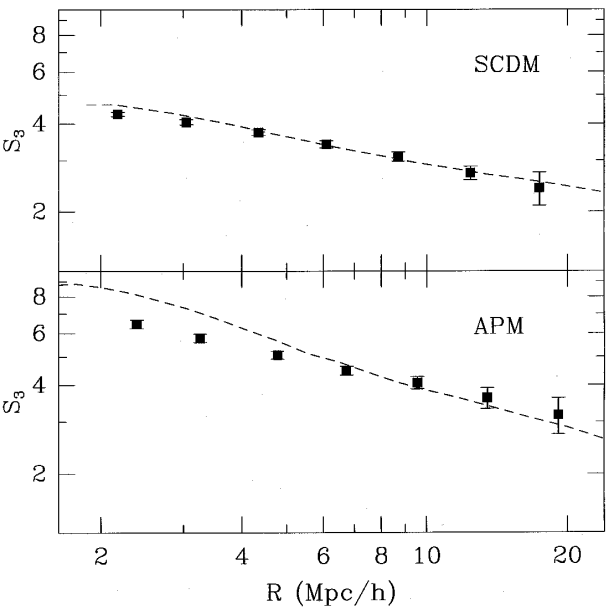

Figure 8. Comparison of the skewness, $S_3(R)$, in the simulated box (dashed lines) with the results inverted from the corresponding angular mock catalogue (points). The top panel shows the $\Gamma=0.5$ SCDM3(a) model, while the bottom panel corresponds to the APM3(a) simulation.

on scales $\lesssim 2^\circ$ and tend to produce smaller values of the projected amplitudes s_3 and s_4. Secondly, the simple hierarchical model for projections commonly used in the literature (e.g., by Groth & Peebles 1977 and Fry & Peebles 1978) is not accurate on quasi-linear scales, as was indicated in Bernardeau (1995). These two effects compete with each other, and it is not clear how the projection model should be improved to allow a better reconstruction.

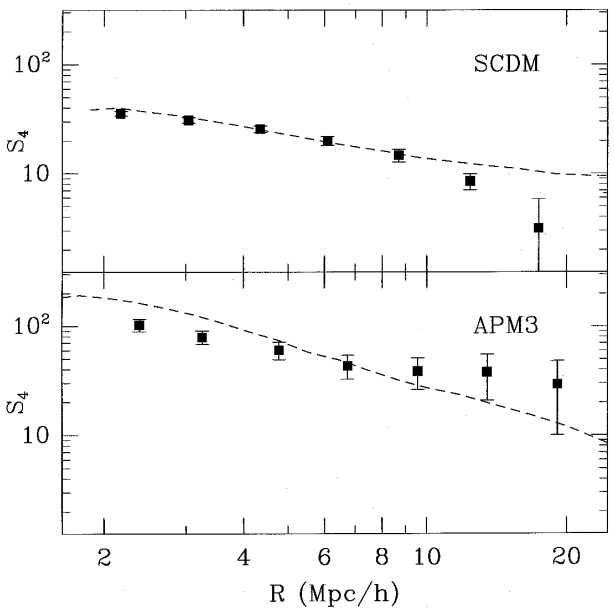

Figure 9. Comparison of the kurtosis, $S_4(R)$, in the simulated boxes (dashed lines) with the results obtained from the angular catalogues (as in Fig. 8).

5 RECOVERY OF THE POWER SPECTRUM

BE93 and BE94 developed an iterative technique to numerically invert Limber's (1954) equation, which relates a measure of clustering in 2D to an integral of the 3D power spectrum multiplied by the survey selection function. BE93 used the measured angular correlation function of the APM Survey, $w(\theta)$, to obtain an estimate of the 3D power spectrum, whilst the 2D power spectrum, $P_2(k)$, was used in BE94. An estimate of the real space correlation function has also been made in the same way (Baugh 1996).

This algorithm for the numerical inversion of Limber's equation does not rely upon the initial form chosen for the power spectrum, and it can reveal features that would be difficult to parametrize in a simple way. The technique is numerically stable, unlike the use of Mellin transforms which involves differentiation of noisy quantities (Fall & Tremaine 1977), and it has been shown to converge rapidly to stable solutions (BE93).

The integral equation relating $w(\theta)$ to the 3D power spectrum, $P(k)$, is given by (BE93; see Peacock 1991 for the non-relativistic form)

$$w(\omega)=\int_0^\infty P(k)\,kg(k\omega)\,\mathrm{d}k, \tag{5}$$

where the angular variable is $\omega=2\sin(\theta/2)$, and the kernel function is an integral over the survey selection function

$$g(k\omega)=\frac{1}{2\pi}\,\frac{1}{(\mathcal{N}\Omega_s)^2}\int_0^\infty \frac{F(x)}{(1+z)^\alpha}\left(\frac{\mathrm{d}N}{\mathrm{d}z}\right)^2\frac{\mathrm{d}z}{\mathrm{d}x}\,J_0(k\omega x)\,\mathrm{d}z, \tag{6}$$

where $F(x)$ depends upon the cosmological model (see Peebles 1980, section 50), and Ω_s is the solid angle of the survey. The time evolution of the power spectrum is parametrized as $P(k,z)=P(k)/(1+z)^\alpha$, where $\alpha=0$ corresponds to the pattern of clustering being fixed in comoving coordinates, which is the case we use in this paper. This is a necessary oversimplification, as we have an observed quantity that is a function of only one variable. Furthermore, the median redshift of the APM Galaxy Survey is $z_m\sim0.12$, and the corrections for redshift evolution are small.

The redshift distribution of survey galaxies is parametrized as (BE93):

$$\left(\frac{\mathrm{d}N}{\mathrm{d}z}\right)\mathrm{d}z=\frac{3\mathcal{N}(m)\,\Omega_s}{2z_c^3}\,z^2\exp\left[-\left(\frac{z}{z_c}\right)^{3/2}\right]\mathrm{d}z, \tag{7}$$

with the median redshift given by

$$z_m=1.412z_c=0.016(b_J-17)^{1.5}+0.046 \tag{8}$$

for apparent magnitudes $b_J\geq17$. This form was chosen to provide a fit to the redshift distribution in the Stromlo/APM survey (Loveday et al. 1992) and to the fainter surveys of Broadhurst, Ellis & Shanks (1988) and of Colless et al. (1990, 1993). Redshifts have now been measured for galaxies in the magnitude range covered by the APM Survey, $17\leq b_J\leq20$ (Ellis et al. 1996), and the redshift distribution is in good agreement with the form that we have adopted (Efstathiou, private communication).

The rth iteration of the Lucy algorithm gives an estimate of the data of

$$w^r(\omega_i)=\sum_j P^r(k_j)\,g(k_j\omega_i)\,k_j^2\Delta\ln k, \tag{9}$$

which is compared with the 'true' data, $w^0(\theta)$ in order to generate a new estimate of the power spectrum:

$$P^{r+1}(k_j)=P^r(k_j)\,\frac{\sum_i \dfrac{w^0(\omega_i)}{w^r(\omega_i)}\,g(k_j\omega_i)\,\Delta\ln\omega}{\sum_i g(k_j\omega_i)\,\Delta\ln\omega}. \tag{10}$$

The summations have typically 60 logarithmic bins for the data, and 30 logarithmic bins for $P(k)$ in the range $3\times10^{-3}\leq k\leq30\ h\ \mathrm{Mpc}^{-1}$.

5.1 Test of the recovery of $P(k)$

In all cases, unless otherwise stated, we use the mean angular two-point correlation function and its variance in four individual disjoint zones (shown in fig. 2 of BE94) to recover the power spectrum. The results of the inversion of equation (5) are illustrated in Fig. 10 for the two CDM models SCDM3(a) and LCDM3(a), which have power spectra with very different amplitudes and curvatures at a given wavenumber. There is very good agreement in each case, up to the largest wavenumbers sampled in the simulation box in these runs, $k\simeq2\pi/L\simeq0.015\ h\ \mathrm{Mpc}^{-1}$. In Section 6.1 below we present a more detailed comparison for larger scales.

6 MEASURING THE BREAK IN $P(k)$

6.1 Accuracy on large scales

In order to show that the inversion method can accurately recover features at small wavenumbers (large scales), such

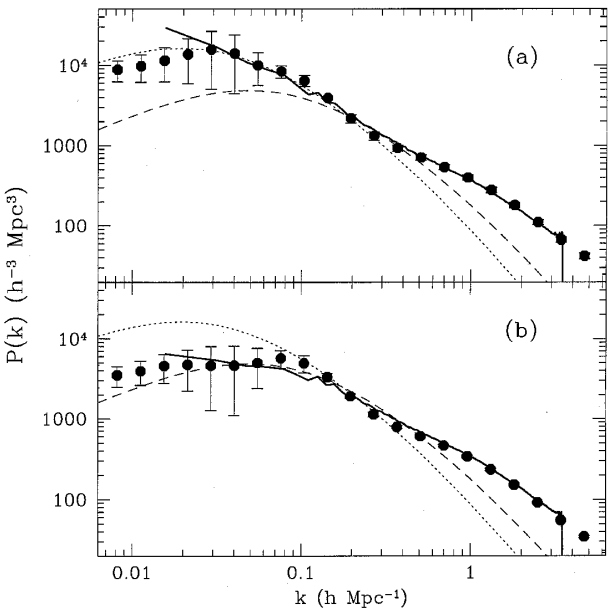

Figure 10. Symbols with error bars show the recovered 3D $P(k)$ from the inversion of equation (5) for maps made from the CDM simulations: (a) LCDM3(a), (b) SCDM3(a). The dotted and dashed lines show for reference the linear power spectra of the LCDM and SCDM models respectively. The solid line in each case shows the non-linear $P(k)$ measured from the simulation.

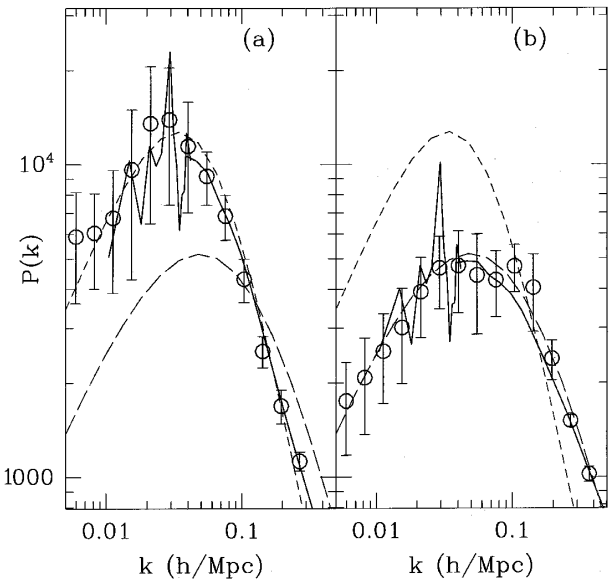

Figure 11. Comparison of the recovered 3D $P(k)$ (points with error bars), from the angular catalogues, with the $P(k)$ from the corresponding 3D simulation (continuous line). The left-hand panel shows the results for APM2(a), and the right-hand panel shows those for SCDM2(a). The long- and short-dashed lines correspond to the $\Gamma=0.5$ linear CDM $P(k)$ and the APM linear power spectrum respectively.

as the break in $P(k)$, we now concentrate on the largest volume simulations, with a box size of $L=600\,h^{-1}$ Mpc (see Table 1). We study a single mock angular map from SCDM2(a) and APM2(a), with the same phase correlations and position for the observer. Fig. 11 shows a comparison of the initial linear $P(k)$ (dashed lines) with the non-linear $P(k)$ in 3D from the full box (continuous line) for both: (a) SCDM (right-hand panel) and (b) the APM model (left-hand panel). Note how even the $P(k)$ measured in the 3D box has large fluctuations at small k and, in particular, a large spike at $k\simeq 0.03\ h$ Mpc^{-1}. This is due to the small number of modes available to estimate $P(k)$ on these scales with the FFT technique. These estimates have not been averaged in bins, and the initial spectrum amplitudes are drawn from a Gaussian distribution (and are not set equal to the mean). The mode where this spike is located only corresponds to $nx=2$ $ny=2$ $nz=0$, so that there are few modes to average over. This is seen in both the APM and CDM $P(k)$ in this plot, due to these simulations being set up with the same phase distributions.

On large scales in Fig. 11 we plot the power spectrum at the individual Fourier modes. At large wavenumbers we have binned the 3D FFT estimation for clarity. The recovered $P(k)$ from the angular two-point function (points with error bars) shows excellent agreement with the original $P(k)$. Hence the volume of a single N-body box ($L=600\,h^{-1}$ Mpc) is large enough to simulate and recover large-scale features in $P(k)$, even at $k\sim 0.01\ h$ Mpc^{-1}.

It is clear from this figure alone that there is a singificant measurement of the break of the power spectrum. To make this more qualitative, we now turn to the local slope of $P(k)$.

We want to focus in more detail on the shape of the power spectrum by estimating the local logarithmic slope:

$$n(k)\equiv\frac{\mathrm{d}\,\log P(k)}{\mathrm{d}\,\log k}. \tag{11}$$

To do a numerical estimation, we first bin the $P(k)$ data and use standard polynomial interpolation and numerical differentiation (e.g. Press et al. 1992) in logarithmic space. The error in the slope is obtained assuming no spread in k:

$$\Delta n(k)\simeq\frac{\mathrm{d}\,\Delta P(k)/P(k)}{\mathrm{d}\,\log k}. \tag{12}$$

This approach seems to work well in the mock maps and avoids spreading the systematic errors coming from the sampling variance, which typically introduces a larger uncertainty in the amplitude of the correlations than in their shape (see fig. 4 in Baugh et al. 1995).

Fig. 12 shows the results for single realizations of the SCDM and APM models for two different box sizes: SCDM2(a) and AMP2(a) with box size $L=600\,h^{-1}$ Mpc, and SCDM3(a) and APM3(a) which have a box size of $L=400\,h^{-1}$ Mpc. The largest scales sampled in each pair of simulations correspond to wavenumbers of $k\simeq 2\pi/L\simeq 0.01\,h$ Mpc^{-1} and $k\simeq 0.015\ h$ Mpc^{-1} respectively for the $L=600$ and $400\,h^{-1}$ Mpc boxes. The smallest scales sampled are limited by the Nyquist frequency of the FFT grid (of size N_g): $k\simeq N_g\pi/L$, or for large enough N_g by the numerical resolution (ϵ in Table 1).

Fig. 12 shows that the recovered slope matches closely that obtained directly in 3D, both in the non-linear ($k>0.2$

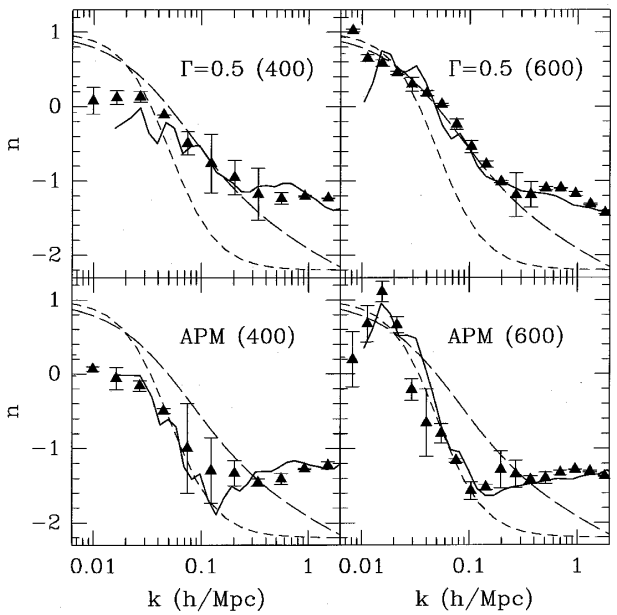

Figure 12. Comparison of the recovered 3D local slope $n(k)$ (points with error bars), from the angular catalogues, with the slope in the corresponding 3D power spectrum (continuous line). The long- and short-dashed lines correspond to the $\Gamma=0.5$ linear CDM model and the APM linear model respectively. The left and right panels show the results in the small (400 h^{-1} Mpc) and large (600 h^{-1} Mpc) boxes. The top and bottom panels correspond to SCDM and APM simulations respectively.

h Mpc^{-1}) and linear ($k<0.1\,h$ Mpc^{-1}) regimes. The particular realizations of the smaller boxes shown in Fig. 12 have a flatter slope on large scales in 3D than the corresponding linear spectrum due to finite-volume effects. This effect is also reproduced in the recovered slopes.

The break in $P(k)$ corresponds to $n=0$, and is well traced within the errors in the larger boxes.

6.2 Implications for the APM power spectrum

Table 2 shows the values of $P(k)$ recovered from the two-point correlations in the APM angular Galaxy Catalogue. These are essentially the same as in fig. 7 of BE93, although there are small differences corresponding to a different number of iterations in the Lucy algorithm (chosen here to provide the minimum χ^2 match to the angular correlation function). Figs 13 and 14 illustrate the implications of our findings for the power spectrum recovered from the APM. Fig. 13 shows the reconstructed slope in the APM Galaxy power spectrum, while Fig. 14 shows the corresponding $P(k)$. Symbols with error bars correspond to the mean and variance in four individual disjoint zones (shown in Table 2). The break at $n=0$ is found to lie at $k=0.02$–0.06 h Mpc^{-1} (between the vertical dotted lines in the figure). This can also be shown directly in Fig. 14, where $P(k)$ shows a significant break on similar scales (also bounded by dotted lines). Note that the error bars are comparable in the mock and the real catalogues.

The power spectrum recovered from the mock catalogues agrees well with the $P(k)$ measured from the unprojected simulation box, indicating that the volume of a single box ($L=600\,h^{-1}$ Mpc) is large enough to realize and recover a break on scales around $k\simeq 0.05\,h$ Mpc^{-1}, without any finite-volume effects. Thus the volume traced by the APM Survey (which extends radially well beyond 600 h^{-1} Mpc) is large enough to allow a measurement of the break in the power spectrum, $n=0$.

In an extensive analysis of the systematic errors involved in plate matching, Maddox et al. (1996) have placed an upper limit of $\delta w(\theta)\sim 1\times 10^{-3}$ on the likely contribution of the systematic errors to the angular correlations. In Figs 13 and 14 the inversion result using the angular correlation function measured from the full survey is shown as a continuous line. The short-dashed lines in these figures show how this result for the power spectrum changes when an offset of 10^{-3} is subtracted from the angular correlation function in the full APM map. In principle, results from individual zones (symbols with errors in the figures) could be affected more by the zone boundary than results from the full survey,

Table 2. Values of the estimated power spectrum $P(k)$ recovered from measurements in the (real) APM angular galaxy catalogue, corresponding to the mean and error from the variance in four individual disjoint regions in the catalogue. No correction for merged stars has been applied (final amplitude should be 10 per cent higher).

k $hMpc^{-1}$	$P(k)$ $(h^{-3}Mpc^3)$	$\Delta P(k)$ $(h^{-3}Mpc^3)$
0.0032	7198	4345
0.0043	6891	3278
0.0060	5805	2126
0.0082	5386	1543
0.0113	6158	1620
0.0155	8134	2026
0.0213	10174	2803
0.0292	10251	3682
0.0401	9821	3232
0.0551	10776	523
0.0757	9440	1770
0.104	6299	1383
0.143	3358	590
0.196	1754	173
0.270	1048	58
0.371	675	51
0.509	451	41
0.700	309	33
0.961	214	24
1.32	146	16
1.81	96.7	8.8
2.49	61.4	4.6
3.42	38.1	2.4
4.70	23.8	1.3
6.46	15.1	0.7
8.88	9.63	0.43
12.2	6.19	0.25
16.8	4.15	0.15
23.0	3.05	0.10
31.6	2.42	0.07

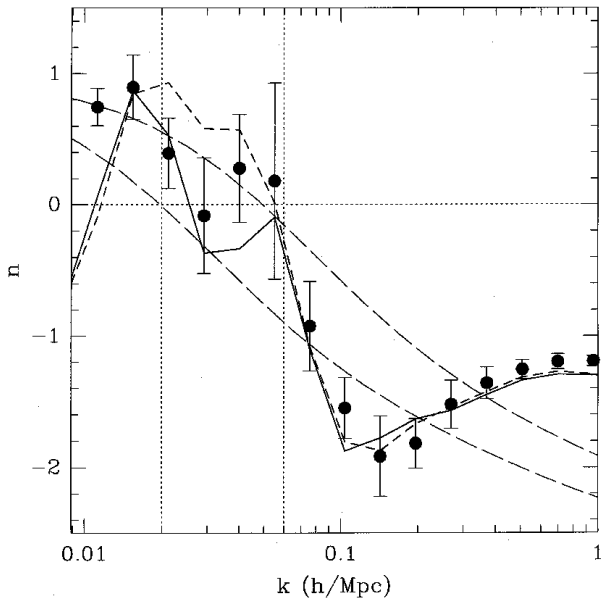

Figure 13. The local slope of the power spectrum estimated from the APM catalogue. Symbols with error bars correspond to the slope estimated in four individual disjoint zones (subsamples). The continuous line is from an inversion of the angular correlation function measured from the full APM map. The short-dashed line corresponds to the inversion after subtracting 10^{-3} from the angular correlation function in the full APM map. The two long-dashed lines correspond to linear CDM models with $\Omega h = 0.5$ (top) and $\Omega h = 0.2$ (bottom).

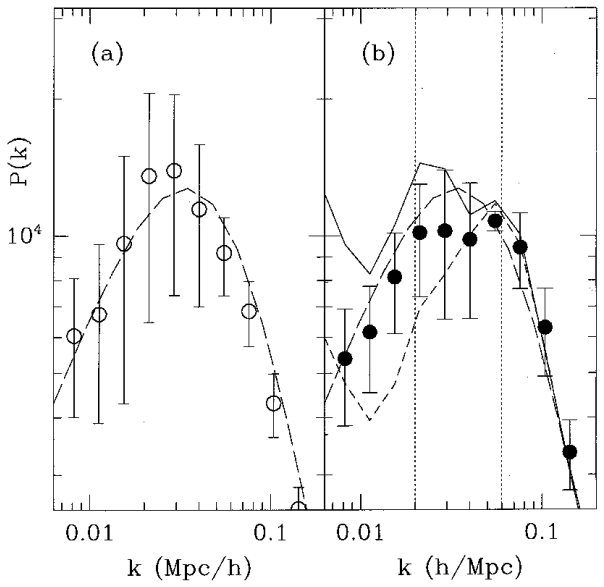

Figure 14. Comparison of the recovered $P(k)$ (points with error bars), from the angular catalogues, with the linear APM model (long-dashed line). Panel (a) corresponds to a mock APM catalogue [APM2(a)]. Panel (b) shows the estimated APM $P(k)$ from measurements in the real galaxy catalogue. In both cases the points and error bars correspond to the mean and variance in four individual disjoint zones (subsamples). The continuous line in panel (b) corresponds to the inverse result obtained using the angular correlation function measured from the full APM map. The short-dashed line corresponds to the inversion result after subtracting an offset of 10^{-3} from $\omega(\theta)$.

although, on the other hand, large-scale noise from plate matching could be more important for the whole survey than for individual zones. For the mock catalogues, the smaller size of individual zones does not seem to introduce important errors at the scales under consideration (e.g. Fig. 12). Thus, while there is no clear reason to prefer the estimate of the power spectrum made from the full survey to that made from the zones, the latter is less likely to be affected by any large-scale plate-matching errors. As the variance from the different zones includes all the above sources of potential error, we take this estimation and variance as our best mean and errors.

Fig. 15 shows the effects of non-linear evolution in the mass power spectrum for the $\Gamma = 0.5$ standard CDM model and for two variants of SCDM with $\Gamma = 0.2$. Again, we use the form of the CDM power spectrum given by Bond & Efstathiou (1984), which is valid for a universe with a small baryon density, $\Omega_B = 0.03$, and we follow the definition of $\Gamma = \Omega h = 0.5$ for SCDM adopted by Efstathiou et al. (1992). For $\Gamma = 0.5$ we show linear-theory power spectra (solid lines) for two different normalizations to the variance in spheres of radius $8\ h^{-1}$ Mpc; the amplitude of temperature fluctuations in the microwave background gives a value $\sigma_8 \simeq 1.2$ (e.g. Stompor, Banday & Gorski 1995; Bunn, Liddle & White 1996), whilst normalization to reproduce the abundance of rich clusters requires $\sigma_8 \simeq 0.50$, virtually independent of the shape of the power spectrum for $\Omega = 1$ (White, Efstathiou & Frenk 1993; Eke, Cole & Frenk 1996). The dashed lines give the corresponding predictions for the non-linear spectra, using the transformation of Peacock & Dodds (1996) rather than that of Jain et al. (1995), which is not so accurate for CDM models (see BG96). The lower set of curves in Fig. 15(c) show a critical-density model with a Hubble constant $H_0 = 50$ km s^{-1} Mpc^{-1}, but with the SCDM transfer function altered by using $\Gamma = 0.2$. The normalization of this curve matches the *COBE* detection, with $\sigma_8 = 0.42$. The upper curves in (c) are for an open model with density parameter $\Omega = 0.2$ and $H_0 = 100$ km s^{-1} Mpc^{-1}. In this case the model is normalized to reproduce the abundance of rich clusters with $\sigma_8 = 1.07$ (Eke et al. 1996).

The APM galaxy power spectrum has been plotted to match the amplitude of the mass power spectrum, dividing the observed amplitude by a bias parameter squared. In the (a) panel, the bias parameters have been chosen to match the galaxy power spectrum to the amplitude of the mass power spectrum at wavenumbers $0.3 \leq k \leq 10\ h$ Mpc^{-1}, whilst in the (b) panel, the match is made at the scale of the break in the APM power spectrum. Panel (c) shows the case for $\Gamma = 0.2$ normalized to small scales. This figure demonstrates the basic problem of the CDM model; the shape of the power spectrum cannot be made to match the observed galaxy power spectrum at both large and small scales, unless some complicated biasing prescription is invoked, in which the bias would need to vary significantly with scale.

6.2.1 *The effect of biasing*

The fluctuations traced by the galaxy distribution might be different, or biased, from the underlying mass fluctuations

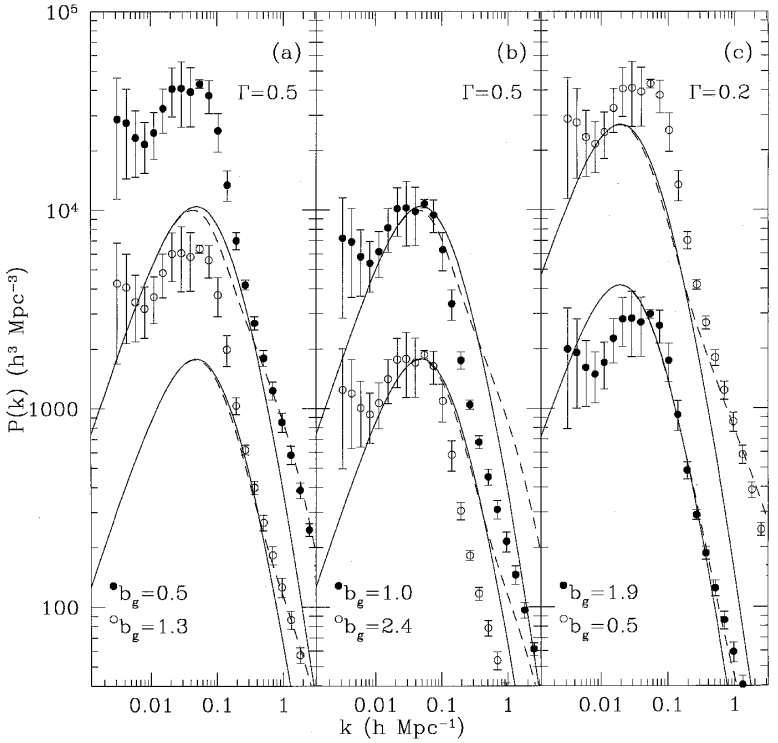

Figure 15. The effects of non-linear evolution on the shape of CDM power spectrum. The solid lines show the linear-theory power spectrum: the lower and upper curves in (a) and (b) are for normalizations of $\sigma_8=0.50$ and 1.21 respectively in the $\Gamma=0.5$ CDM model. The lower solid curve in panel (c) shows a $\Gamma=0.2$ CDM model for a universe with $\Omega=1$ and a Hubble constant of $H_0=50$ km s^{-1} Mpc^{-1}, normalized to match the *COBE* result with $\sigma_8=0.42$. The upper solid curve in panel (c) corresponds to an open universe with $\Omega=0.2$ and $H_0=100$ km s^{-1} Mpc^{-1}, with a normalization that reproduces the abundance of rich clusters, $\sigma_8=1.07$. The dashed curves show the corresponding non-linear power spectra; in this case we have used the transformation of Peacock & Dodds (1996), which is expressed in a form that makes it readily applicable to different cosmological models.

The APM galaxy power spectrum is shown by points with error bars, where we have divided by a bias parameter, b_g, squared (values indicated in the figure) to match the amplitude of the mass spectrum at different scales: (a) the bias parameters have been chosen to match the amplitude of the mass $\Gamma=0.5$ CDM $P(k)$ on small scales $k\gtrsim0.5$; (b) the match is made to the amplitude of the mass $\Gamma=0.5$ CDM spectrum at the scale of the break in the APM power spectrum, $k\simeq0.05$; (c) match to the amplitude of the mass $\Gamma=0.2$ CDM spectrum on small scales, $k\gtrsim0.5$. At small wavenumbers, $k<0.01\ h$ Mpc^{-1}, the estimate of the APM power spectrum is dominated by systematic and random errors in the catalogue.

(e.g. Bardeen et al. 1986). We will argue here that the effect of this biasing is not important for the shape of the APM power spectrum at large scales.

Assume that the (smoothed) galaxy fluctuations δ_g are related to the mass fluctuations δ_m by a local transformation: $\delta_g(x)=F[\delta_m(x)]$, and that this relation can be given as a Taylor series: $F=b_1\delta_m+b_2\delta_m^2+\ldots$. Then the two-point function $\xi_2^g(r)\equiv\langle\delta_g(x)\,\delta_g(x+r)\rangle$ on a scale r will be just given by

$$\xi_2^g(r)=b_1^2\xi_2^m(r)+b_1b_2\langle\delta_m(x)\,\delta_m(x+r)^2\rangle + b_1b_2\langle\delta_m^2(x)\,\delta_m(x+r)\rangle+\ldots, \quad (13)$$

where all further terms are of order 4 or greater in δ_m, and therefore correspond to either higher order correlations, ξ_J, with $J>2$, or higher powers in ξ_2. If δ_m is Gaussian or hierarchical (as in the case for gravitational evolution) the higher order correlations ξ_J are at most of order ξ_2^{J-1}. This means that at large scales, where $\xi_2<1$, the first term is the dominant one, so that only the amplitude but not the shape of the two-point statistics is changed by biasing. This effect has been found in N-body simulations and toy biasing models (Weinberg 1994; Gaztañaga & Lacey 1997, in preparation; Mo, Jing & White 1997).

For the APM power spectrum, a wavenumber around $k\simeq0.1\ h$ Mpc^{-1} corresponds to a top-hat radius of $R\sim\pi/k\simeq30\ h^{-1}$ Mpc. For any reasonable biasing model relating galaxy fluctuations, δ_g, to the underlying matter fluctuations, δ_m, the matter density fluctuations are very small, around $R\simeq30\,h^{-1}$ Mpc. The independent constraints on the normalization of mass fluctuations discussed above give values of around unity for the variance in spheres of radius $8\,h^{-1}$ Mpc. To have rms fluctuations of order unity at $R\simeq30\ h^{-1}$ Mpc would imply $\sigma_8>3$.

Thus, from the above arguments, the small variance on large scales, $R\gtrsim8\ h^{-1}$ Mpc, means that it is reasonable to assume that the galaxy shape of $P(k)$ for $k<0.1\ h$ Mpc^{-1} corresponds to the shape of the underlying linear matter power spectrum. This argument, just based on the smallness of the variance and the hierarchical structure, can also be applied to gravity, as the leading contribution to the correlation functions in perturbation theory is indeed exactly given

by a local transformation (see Fosalba & Gaztañaga 1997, in preparation). This is clearly illustrated in Fig. 12. By comparing the linear and non-linear shape of $P(k)$, one can see that it has not been changed significantly by gravitational evolution on scales where the rms fluctuations are small, i.e., $k < 0.1\ h\ \mathrm{Mpc}^{-1}$.

6.2.2 *Variations of CDM models*

A simple variation of CDM models is to introduce a tilt in the initial power spectrum so that $P(k) = k^{n_0} T(k)$, where $T(k)$ is the transfer function (e.g. Bond & Efstathiou 1984; Bardeen et al. 1986) and n_0 is primordial spectral index, $n_0 \neq 1$. Unless the transfer function $T(k)$ somehow depends strongly on n_0, the local slope of a given tilted CDM model is similar to that of the corresponding standard scale-invariant model (where $n_0 = 1$), given by $n = n_0 + \mathrm{d}\log(T)/\mathrm{d}\log(k)$, with the shift due to the tilted value of n_0. Thus, tilted models can only scale up or down the CDM predictions in Fig. 13, and therefore cannot account for the APM observations.

The measurement of the abundance of deuterium in high-redshift hydrogen clouds is provoking much debate in the literature (e.g. Rugers & Hogan 1996; Tytler, Fan & Burles 1996). Consequently, the baryon density of the Universe is uncertain, and possible values fall in a wider range than was previously accepted. In the limit of a high baryon density (i.e., $\Omega_{\mathrm{B}} \sim 0.1$), the power spectrum of the mass is modified. A full calculation of the transfer function (e.g. Seljak & Zaldarriaga 1996) indicates that the high baryon density introduces features or 'wiggles' into the shape of the power spectrum on large scales (see also Goldberg & Strauss 1997 for a discussion of how these peaks could be used to constrain the value of Ω_{B}). We have used the CMB-fast code of Seljak & Zaldarriaga to compute the shape of the power spectrum in a CDM universe with $\Omega_{\mathrm{B}} = 0.1$ and $\Omega = 1$. The resulting modification of the power spectrum compared with the Bond & Efstathiou (1984) transfer function for $\Omega_{\mathrm{B}} = 0.03$ is insufficient to improve the agreement with the APM power spectrum.

7 CONCLUSIONS

The algorithms tested here successfully recover the power spectrum and higher order cumulants in three dimensions (3D). There are no systematic shifts or biases in the inferred correlations resulting either from the deprojection techniques or from the pocess of projecting the original particle distribution. The 3D variance recovered from angular catalogues is in good agreement with the input model, confirming the results in G95. For higher order correlations the deprojection method studied here, and also used in G94, Gaztañaga & Frieman (1994), G95 and BG96, seems to be adequate, at least for intermediate scales, $20 > R > 6\ h^{-1}$ Mpc, although one would, in principle, expect deviations from the simple hierarchical, according to perturbation theory (Bernardeau 1995). A more detailed analysis of this point is presented elsewhere (see Gaztañaga & Bernardeau 1997).

It is possible to recover the detailed shape of the power spectrum, with error bars similar to those quoted by BE93. As pointed out there (and also in G95), the uncertainties in the selection function do not have much effect on the recovered shape. The deprojection algorithm is able to distinguish sharp features, such as the one for $k \simeq 0.07$–$0.2\ h\ \mathrm{Mpc}^{-1}$ shown in Fig. 13, first remarked upon by BE93. For this range of wavenumbers, the best-fitting CDM model has $\Omega h \simeq 0.2$, as pointed out by Efstathiou et al. (1990b) and Peacock & Dodds (1994). However, the break in the power spectrum in this particular CDM model is broader and at a larger scale than the break in the APM power spectrum.

We have shown that the volume traced by the APM Survey is large enough to allow a significant measurement of the break in the power spectrum, $n = 0$, as found on scales around $k \simeq 0.05\ h\ \mathrm{Mpc}^{-1}$. We have also shown (see Fig. 14) that possible systematic errors involved in the APM plate matching lie within our estimated errors.

Peacock & Dodds (1994) report a break in the power spectrum at a wavenumber of $k \simeq 0.02\ h\ \mathrm{Mpc}^{-1}$ using spectra measured from a range of different surveys. The volumes mapped out by these surveys span a considerable range. We have found that only our largest simulation boxes allow the break to be measured accurately, both in the direct estimation of the power spectrum in 3D and in the recovered spectrum obtained from the projected catalogue. The size of the largest box we use, $L = 600\ h^{-1}$ Mpc, is much greater than the median depth of any of the redshift surveys available to Peacock & Dodds, indicating that finite-volume effects could have altered the shape of the power spectra estimated from individual surveys on large scales (as found in Fig. 12 for the $400\ h^{-1}$ Mpc boxes). Other sources of uncertainty in this type of compilation include the different selection biases applied, the differences in the intrinsic luminosities of the objects selected in the catalogue, and the large sampling variance from the smaller surveys. Furhermore, the linearization process applied to the measured power spectra involves a correction for the distortion of the pattern of clustering by galaxy peculiar velocities (Kaiser 1987), which is both model- and catalogue-dependent (e.g. Smith et al. 1997).

The location of the break that we find in the galaxy power spectrum matches that found in power spectrum of galaxies clusters, both from a compilation based on the Abell catalogue (Einasto et al. 1997) and from a carefully selected redshift sample drawn from the APM Cluster Catalogue (Dalton et al. 1992; Tadros 1996; Tadros & Dalton 1997, in preparation).

The physical interpretation of the break at

$$k_{\mathrm{B}} \simeq 0.05\ h\ \mathrm{Mpc}^{-1} \simeq 150\,\frac{H_0}{c} \tag{14}$$

found in the APM is unclear. We have argued in Section 6.2.1 that the galaxy shape of $P(k)$ for $k < 0.1\ h\ \mathrm{Mpc}^{-1}$ corresponds to the shape in the underlying linear matter power spectrum. For inflationary models with cold dark matter (CDM) the break in the power spectrum at wavenumber k_{B} corresponds to the Hubble radius when the Universe becomes matter-dominated. This is because the amplitude of fluctuations is frozen as they enter the Hubble radius during the radiation-dominated era (see Bond & Efstathiou 1984; Bardeen et al. 1986). The wavelength of the Hubble radius at this epoch is $\lambda_{\mathrm{B}} \sim 10(\Omega h)^{-1}\ h^{-1}$ Mpc

(e.g. Kolb & Turner 1990), where Ω is the total matter density in units of the critical density, which corresponds to a wavenumber of $k_{\rm B} \simeq 0.1(\Omega h)\ h\ {\rm Mpc}^{-1}$. Thus, for CDM-like models, the range of the scales we find for the break in the APM, $k = 0.02$–$0.06\ h\ {\rm Mpc}^{-1}$, implies $0.2 \lesssim \Omega h \lesssim 0.6$. To be more precise, we perform a χ^2 fit to the CDM models in Bond & Efstathiou (1984) using the four APM $P(k)$ points in the range $k = 0.02$–$0.06\ h\ {\rm Mpc}^{-1}$ to find $\Omega h \simeq 0.45 \pm 0.10$ ($\Omega h = 0.2$ produces a $\chi^2 \simeq 9$, while $\Omega h = 0.4$ gives $\chi^2 \simeq 1.3$). Thus the case $\Omega = 1$ requires $h \simeq 0.45 \pm 0.10$, while an open universe or one with a non-zero cosmological constant, Λ, can accommodate other values of the Hubble constant h. For purely relativistic dark matter, like neutrinos, the scale at which the amplitude of fluctuations are damped is typically larger than for CDM, corresponding to the Hubble radius when the universe becomes non-relativistic. For these models the measured break yields correspondingly larger values for Ωh.

As shown in Fig. 13, the sharp change in the local slope of the APM at $k \simeq 0.05$–$0.1\ h\ {\rm Mpc}^{-1}$ is not compatible with any CDM model, which has a broader peak. Note that in Fig. 13, the results are independent of uncertainties in the overall normalization or in any linear bias that may be applied, unlike Fig. 15. We have also shown that non-linear evolution is not sufficient to modify the shape of the linear CDM power spectrum to provide a good match to the shape of the observed APM spectrum.

We have argued in Section 6.2.2 that simple variations of CDM models, such as tilted or higher $\Omega_{\rm B}$ models, cannot account for the APM observations. Models in which a large fraction of the matter is relativistic (such as mixed dark matter) are more likely to match this type of sharp feature. The scale found here for the break, around $k \simeq 0.05\ h\ {\rm Mpc}^{-1}$, could give interesting constraints for these models.

ACKNOWLEDGMENTS

We thank George Efstathiou for supplying us with a copy of the P^{3}M code. We also thank Gavin Dalton, Radek Stompor and Carlos Frenk for help and stimulating discussions. CMB acknowledges receipt of a PPARC research assistantship and support from CESCA (HCM/EC grant) during a visit to the Institut d'Estudis Espacials de Catalunya. EG acknowledges support from CSIC, BGICYT (Spain), project PB93-0035 and CIRIT (Generalitat de Catalunya), grant GR94-8001.

REFERENCES

Bardeen J. M., Bond J. R., Kaiser N., Szalay A. S., 1986, ApJ, 304, 15
Baugh C. M., 1996, MNRAS, 280, 267
Baugh C. M., Efstathiou G., 1993, MNRAS, 265, 145 (BE93)
Baugh C. M., Efstathiou G., 1994, MNRAS, 267, 323 (BE94)
Baugh C. M., Gaztañaga E., 1996, MNRAS, 280, L37 (BG96)
Baugh C. M., Gaztañaga E., Efstathiou G., 1995, MNRAS, 274, 1049
Barnardeau F., 1995, A&A, 301, 309
Bond J. R., Efstathiou G., 1984, ApJ, 285, L45
Boschan P., Szapudi I., Szalay A. S., 1994, ApJS, 93, 65
Broadhurst R. S., Ellis R. S., Shanks T., 1988, MNRAS, 235, 827
Bunn E. F., Liddle A. R., White M., 1996, Phys. Rev. D, 54, R5917
Cole S., Fisher K. B., Weinberg D. H., 1995, MNRAS, 275, 515
Colless M., Ellis R. S., Taylor K., Hook R. N., 1990, MNRAS, 244, 408
Colless M., Ellis R. S., Broadhurst T. J., Taylor K., Peterson B. A., 1993, MNRAS, 261, 19
Dalton G. B., Efstathiou G., Maddox S. J., Sutherland W. J., 1992, ApJ, 390, L1
Efstathiou G., Davis M., Frenk C. S., White S. D. M., 1985, ApJS, 57, 241
Efstathiou G., Kaiser N., Saunders W., Lawrence A., Rowan-Robinson M., Ellis R. S., Frenk C. S., 1990a, MNRAS, 247, 10P
Efstathiou G., Sutherland W. J., Maddox S. J., 1990b, Nat, 348, 705
Efstathiou G., Bond J. R., White S. D. M., 1992, MNRAS, 258, 1P
Einasto J. et al., 1997, Nat, 385, 139
Eke V. R., Cole S., Frenk C. S., 1996, MNRAS, 282, 263
Ellis R. S., Colless M., Broadhurst T., Heyl J., Glazebrook K., 1996, MNRAS, 280, 235
Fall S. M., Tremaine S., 1977, ApJ, 216, 682
Fisher K. B., Davis M., Strauss M. A., Yahil A., Huchra J., 1993, ApJ, 402, 42
Fry J. N., Peebles P. J. E., 1978, ApJ, 221, 19
Gaztañaga E., 1994, MNRAS, 268, 913 (G94)
Gaztañaga E., 1995, ApJ, 454, 561 (G95)
Gaztañaga E., Bernardeau F., 1997, A&A, in press
Gaztañaga E., Frieman J. A., 1994, ApJ, 437, L13
Goldberg D. M., Strauss M., 1997, ApJ, submitted
Groth E. J., Peebles P. J. E., 1977, ApJ, 217, 385
Gunn J. E., Weinberg D. H., 1995, in Maddox S. J., Aragon-Salamanca A., eds, Wide Field Spectroscopy and the Distant Universe. Proceedings of 35th Herstmonceux Workshop, World Scientific Press, Singapore
Hamilton A. J. S., Kumar P., Lu E., Matthews A., 1991, ApJ, 374, L1
Jain B., Mo H. J., White S. D. M., 1995, MNRAS, 276, L25
Kaiser N., 1984, ApJ, 284, L9
Kaiser N., 1987, MNRAS, 227, 1
Kolb E. W., Turner M. S., 1990, The Early Universe. Addison-Wesley, New York
Limber D. N., 1954, ApJ, 119, 655
Loveday L., Peterson B. A., Efstathiou G., Maddox S. J., 1992, ApJ, 390, 338
Maddox S. J., Sutherland W. J., Efstathiou G., Loveday L., Peterson B. A., 1990a, MNRAS, 243, 692
Maddox S. J., Efstathiou G., Sutherland W. J., 1990b, MNRAS, 246, 433
Maddox S. J., Efstathiou G., Sutherlands W. J., Loveday L., 1990c, MNRAS, 242, 43P
Maddox S. J., Efstathiou G., Sutherlands W. J., Loveday L., 1996, MNRAS, 283, 1227
Mo H. J., Jing Y. P., White S. D. M., 1997, MNRAS, 284, 189
Peacock J. A., 1991, MNRAS, 253, 1P
Peacock J. A., Dodds S. J., 1994, MNRAS, 267, 1020
Peacock J. A., Dodds S. J., 1996, MNRAS, 280, L19
Peebles P. J. E., 1980, The Large Scale Structure of the Universe. Princeton Univ. Presss, Princeton
Press W. H., Teukolsky S. A., Vetterling W. T., Flannery B. P., 1992, Numerical Recipes. Cambridge Univ. Press, Cambridge
Rugers M., Hogan C. J., 1996, AJ, 111, 2125
Saunders W. et al., 1991, Nat, 349, 32
Seljak U., Zaldarriaga M., 1996, ApJ, 469, 437
Smith C., Klypin A., Gross M., Primack J., Holtzman J., 1997, MNRAS, submitted (astro-ph/9702099)
Stompor R., Banday A. J., Gorski K. M., 1995, MNRAS, 277, 1225

Tadros H., 1996, PhD thesis, Univ. Oxford
Tadros H., Efstathiou G., 1996, MNRAS, 282, 1381
Tytler D., Fan X. M., Burles S., 1996, Nat, 381, 207
Vogeley M. S., Park C., Geller M. J., Huchra J. P., 1992, ApJ, 391, L5
Weinberg D. H., 1995, in Maddox S. J., Aragon-Salamanca A., eds, Wide Field Spectroscopy and the Distant Universe. Proceedings of the 35th Herstmonceux Conference. World Scientific Press, Singapore
White S. D. M., Efstathiou G., Frenk C. S., 1993, MNRAS, 262, 1023